Journal of Autonomous Intelligence (2024) Volume 7 Issue 5
doi: 10.32629/jai.v7i5.1578

ORIGINAL RESEARCH ARTICLE

Design of an affordable hybrid brain-computer interface to control robotic devices

Yih-Choung Yu[1,*], Haley Garrison[2], Brandon Smith[3], Ashley Goreshnik[4], Alexandria Battison[5], Lisa Gabel[6]

[1] *Department of Electrical and Computer Engineering, Lafayette College, Easton, PA 18042, USA*

[2] *KioWare Kiosk Software, York, PA 17401, USA*

[3] *Modern Technology Solutions, Inc., Alexandria, VA 22312, USA*

[4] *School of Medicine, Yale University, New Haven, CT 06510, USA*

[5] *Cold Spring Harbor Laboratory, Cold Spring Harbor, NY 11724, USA*

[6] *Department of Psychology and Neuroscience Program, Lafayette College, Easton, PA 18042, USA*

*** Corresponding author:** Yih-Choung Yu, yuy@lafayette.edu

ABSTRACT

Brain-computer interfaces (BCIs) are devices that utilize neural activity as the foundation for an alternate method of communication or control of external devices. BCIs establish a connection between natural electrophysiological signals regularly occurring in the brain and desired computerized outputs. Instead of relying on natural neuromuscular outputs, BCIs produce artificial outputs, such as movements or navigation commands, capable of controlling robotic devices. The use of BCIs in robotic control holds significant promise for assisting individuals with motor disabilities in various applications, such as exploration, home assistance, or control of an electric wheelchair, thereby fostering greater independence in their daily activities. This paper presents the design of a hybrid BCI tailored for controlling a variety of robotic devices, including a quadcopter, wheeled robot, and wheelchair, by modifying the control scheme of the BCI. An inexpensive electroencephalogram (EEG) headset was employed to capture occipital alpha waves, frontal muscular artifacts, and gyroscope signals indicating head movements. These signals were wirelessly transmitted to a host computer, where signal processing algorithms were implemented to process the acquired signals and extract possible features to interpret the user's intents as control commands to navigate robotic devices. The response speed and accuracy of the BCI design for robot navigation were recorded and analyzed to evaluate both the performance of the design and the effectiveness of user training. The results support the idea that this cost-effective BCI design can effectively control various robotic devices with minimal adjustments to the control scheme, thus reducing the need for major design changes and user training.

Keywords: hybrid BCI; asynchronous BCI; robot navigation; EEG signal processing

ARTICLE INFO

Received: 5 February 2024
Accepted: 21 March 2024
Available online: 13 August 2024

1. Introduction

Brain-computer interfaces (BCIs) are communication systems that offer an alternate means of motor control and communication, especially for those with severe motor impairments and disabilities. BCIs bypass the peripheral nervous system by acquiring brain activity signals, analyzing them to detect certain patterns from these signals, and translating the patterns to pre-defined commands to control external devices. By way of a neuro-feedback loop, users learn to modulate their neural signals to control a specific computerized paradigm. Ultimately these devices enable individuals who suffer from motor impairment to regain some degrees of autonomy, possibly enhancing their quality of life[1].

Applications of BCI devices have been rapidly expanding in various areas in recent years, driven by advances in computational power, sensor technologies, and mobile devices. Shih et al.[2] illustrated the usefulness of BCI devices in rehabilitation by controlling cursor movements on computer screens, navigating wheelchairs, and manipulating robotic arms. Hehenberger et al.[3] conducted a thorough longitudinal study on the performance of a tetraplegic participant competing in a computer game race with a BCI. Results from this study suggest that the participant's performance, both in terms of class separability in the calibration data and in the game, was significantly improved through regular training.

Xu et al.[4] designed a hybrid BCI device to control a robot arm for selecting and grasping objects in a 3D environment with obstacles. The 2D motion of the robot arm for object searching was controlled by imaginary hand movements of the participants, detected from the noninvasive EEG signals. Information about objects was captured in video using a USB camera mounted on the gripper. The video was displayed on the computer monitor to the participants for object selection. After an object was selected by the participant's eye gazing, captured by an eye tracker, the information of the selected object was transmitted to the computer to control the robot arm for object grasping automatically. Their successful results support the feasibility of human operation to control prosthetic limbs using a non-invasive BCI device.

Bai et al.[5] presented a hybrid BCI system to improve spelling accuracy and speed by simultaneously eliciting and detecting the P300 evoked potential and the steady-state visual evoked potential (SSVEP) using a frequency-enhanced paradigm consisting of alphabets and symbols arranged in a 6-by-6 layout. The rows and columns of the paradigm flash in a pseudorandom sequence at specific frequencies ranging from 6.0 to 11.5 Hz, with an increment of 0.5 Hz, to stimulate the P300 and SSVEP event-related potentials. The P300 potential was detected from the EEG measurements using a signal processing algorithm that combines wavelet and support vector machine techniques, while the SSVEP was detected using an ensemble task-related component analysis method. The two detected scores, related to the potential events, were passed into the total weight controller to determine the possible alphabet or symbol selected by the user. Testing of this BCI speller among 10 participants resulted in a high accuracy of 94.29%.

Utilizing BCI systems to control robotic devices has several significant real-world applications to assist patients with severe motor disabilities[6]. Numerous successful developments of using BCIs in assistive devices have been reported over the last decade. For example, Li et al.[7] designed a wheelchair with a wireless digital-to-analog converter; that can be navigated by a P300-based BCI system. Sellers et al.[8] reported multi-year successful experiences, in which a patient with severe motor disabilities communicated with people and conducted literature search on a daily basis using a BCI communication device. Ai et al.[9] controlled a robotic arm to perform reaching and grasping of multiple objects in an unstructured environment using an SSVEP-based BCI system, eliminating the need for users to switch their gaze between the stimulus interface on the computer screen and the actual scene during operation. This allowed users to easily sense the target's location while gazing at the stimuli, enabling them to achieve the assigned targets with better accuracy, more efficient movement trajectories, and shorter operation times compared to the performance reported with traditional designs. These successful designs provide patients opportunities to regain some degrees of independence, and thus improve the quality of their daily life.

Several BCIs have been successfully developed to control wheelchairs over the last decade. These designs can be classified as synchronous BCI and asynchronous BCI, depending on how the brainwaves of interest are produced[10]. For a synchronous BCI, the user's brainwaves are produced within a certain time window in response to a series of pre-defined stimuli. For example, Li et al.[7] created a paradigm with navigation commands to control the wheelchair's movements, allowing users to select directions by eliciting P300 potentials. These are positive potential deflections in ongoing brain activity, occurring roughly 300 ms after the random occurrence of a desired target stimulus among non-target stimuli. The direction of movement, determined by the user's gaze and P300 responses, was then transmitted to the wheelchair's drive

system via a wireless D/A converter for control. Chen et al.[11] describes a steady state visual evoked potential based BCI system (SSVEP, visually evoked by a stimulus modulated at a fixed frequency and occur as an increase in EEG activity at the stimulus frequency) that controls the operations of an electrical wheelchair, such as forward, reverse, left, right, and stop. Synchronous BCIs allow the inclusion of more navigation and control commands in the design. They require less training time, and their performance is usually more accurate than that of asynchronous BCIs. For these reasons, synchronous BCIs have been successfully employed in controlling many BCI-controlled mobile robots.

For an asynchronous BCI, brainwaves are produced by mental activities, such as motor imagery and mental math counting; thus, no external stimuli are needed. Yu et al.[12] proposed an asynchronous control paradigm based on sequential motor imagery (sMI). By sequentially imagining left- and right-hand movements, subjects can complete four sMI tasks in an asynchronous mode, which are then encoded to control six steering functions of a wheelchair: moving forward, turning left, turning right, accelerating, decelerating, and stopping. Aljalal et al.[13] developed an asynchronous BCI for robot navigation by classifying the user's mental states, specifically left-hand and right-hand motor imagery (MI), from the EEG signals. Common spatial pattern filtering combined with band power calculation were applied to form feature vectors. Linear discriminant analysis was employed to classify the mental states. Based on the combination of the current and new mental states, the system can produce four motion commands: going forward, turning left, turning right, and stopping, to navigate the robot. Asynchronous BCIs don't rely on external stimuli to activate the brainwaves of interest. It usually takes a shorter time to produce the navigation and control commands from an asynchronous BCI than from a synchronous BCI. Therefore, asynchronous BCIs are preferred for mobile robot navigation as timing is critical in this type of application[14]. However, two challenges limit the popularization of these designs. The EEG acquisition systems used in both designs were expensive. Also, training a user to successfully use a sensorimotor rhythm based BCI is usually time-consuming[15,16].

This paper presents a novel design for a hybrid BCI system. The system utilizes the occipital EEG alpha wave associated with eye open and closure, frontal muscular artifacts from eye blinking, and motion signals from head rotations. These signals are employed to navigate three individual robotic devices—a quadcopter, a wheel robot, and a full-size wheelchair—through a host computer. An inexpensive wireless EEG headset with a gyroscope function (EPOC, EMOTIV System, San Francisco, CA) is used in the system for signal acquisition, making the BCI more affordable for a wider range of users. Since all the signals required to operate the BCI are naturally occurring during human activities, minimal training time is needed for effective operation. Consequently, this new design could be more accessible to a broader audience. Moreover, using the same BCI device to control various robotic devices allows users to operate these devices without requiring additional training.

2. Design of the BCI system

The configuration of the hybrid BCI system is illustrated as a feedback loop, shown in **Figure 1**, consisting of four main components: signal acquisition and processing, feature extraction and classification, navigation scheme, and visual feedback. The functions of these components are described in the following.

2.1. EEG headset for signal acquisition

The Emotiv EPOC EEG wireless headset (EPOC, EMOTIV System, San Francisco, CA) was used as the signal acquisition device in this hybrid BCI system. This headset contains 14 fixed electrode positions based on the international 10–20 system, a two-axis gyroscope, and 2 references. The locations of these sensors on the scalp are illustrated in **Figure 2**[17]. Signals from the occipital lobe (indicated as O1 and O2 in **Figure 2**), the frontal lobe (indicated as AF3 and AF4 in **Figure 2**), and the gyroscope associated with head

rotation were sampled at a rate of 128 Hz. These signals were streamlined wirelessly to a host PC to be processed for feature extraction and classification. The BCI system detects specific features from a user's neural signals that are associated with their specific intentions and then sends the appropriate commands to control the external device, such as the quadcopter, wheeled robot, or wheelchair.

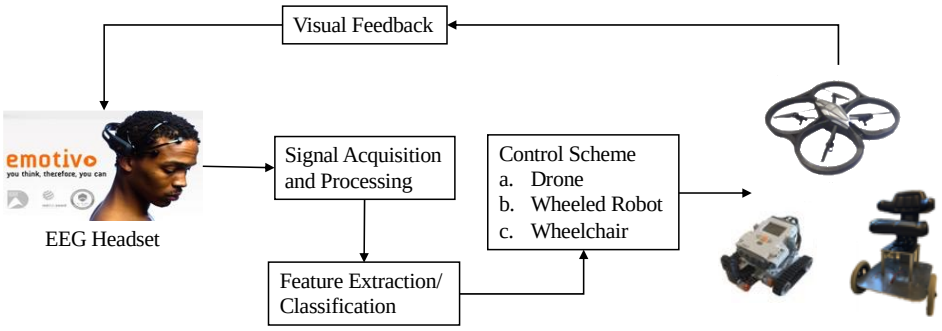

Figure 1. Configuration of the overall BCI System. one platform that can be used for wheeled robot, wheelchair, and quadcopter navigation without major design changes.

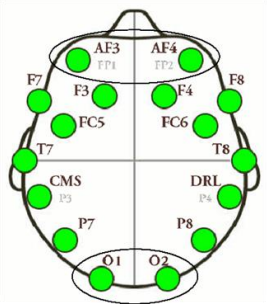

Figure 2. Placement of electrodes on the headset in the Emotiv EPOC system. Signals obtained from the circled locations (AF3, AF4, O1 and O2) were used for the BCI systems. Picture from (Emotiv Systems Inc.)[17]

2.2. Feature extraction and classification

The signals acquired from the EPOC EEG wireless headset were processed to extract the features that reflect the user's intent. The specific intentions employed to control the robotic devices included eye open/closure, eye blinking, and head rotation.

2.2.1. Detection of eye open and close

The experimental results in Tran et al.[16] suggested that eye closure resulted in a detectable voltage rise in EEG waves between 8 and 13 Hz in people with spinal cord injury. EEG alpha waves, acquired by the EPOC EEG wireless headset from the occipital lobe (O1 and O2 electrodes in **Figure 2**), were processed on the host PC to detect eye open and close. The signal processing algorithm, implemented in Java on the host PC, is illustrated in the block diagram in **Figure 3**[17].

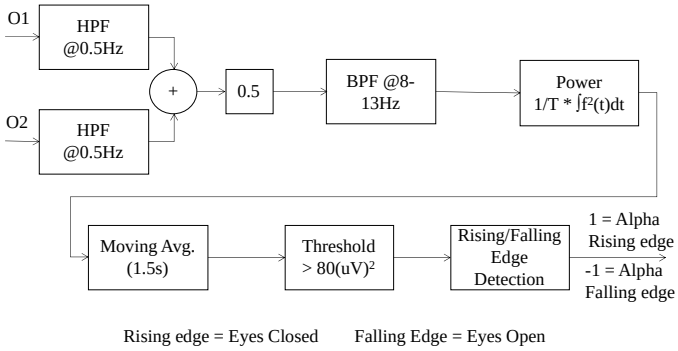

Figure 3. Block diagram of feature extraction and classification for eye open and close using the EEG alpha wave from the occipital lobes[17].

A highpass filter with a cutoff frequency of 0.5 Hz is included in the EPOC EEG headset to remove the DC offset from the EEG signal from each electrode. Signals from O1 and O2 were averaged to enhance the signal-to-noise ratio. Since the EEG alpha wave of interest for eye open and close is in the frequency range of 8–13 Hz, a 4th-order Butterworth bandpass filter with a frequency band of 8–13 Hz was applied to the average signal to remove the noise beyond this frequency range. A Butterworth filter was chosen for the advantage of maximum flatness in the passband with a gain close to one. The order of the filter was determined to provide a sufficiently steep cutoff to retain the alpha band and reject other frequencies while avoiding the time complexity of higher-order filters[10]. A sample set of EEG data from O1 and O2 electrodes after bandpass filtering is shown in **Figure 4a**. Data were obtained from a participant performing eye opening during the first 5 s and eye closing for the next 5 s in an experiment. Higher voltage amplitudes due to eye closure were observed in the second half of the graph.

The bandpass filtered EEG alpha wave was used to calculate the averaged power in discrete time as:

$$P(n) = \frac{1}{T}\sum_{k=n-N}^{n} f(k)^2 \Delta t \tag{1}$$

where $f(k)$ is the k-th sample of the filtered EEG (in the form of voltage) sample, $\Delta t = \frac{1}{128}$ s is the sampling period and $N = 128T$ samples is the window size with $n \geq N$. The period $T = \frac{1}{10.5}$ s was determined by assuming that the filtered signal is an intermediate frequency sinusoid, where 10.5 Hz is the average of 8 and 13 Hz[10]. The averaged power calculated by using the bandpass filtered EEG signal in **Figure 4a** is illustrated in **Figure 4b**, in which the rising power related to eye closure is visible. However, it is difficult to detect eye closure directly by using the average power due to the fluctuations in the waveform. Therefore, the averaged power was further processed by a 1.5-second moving average filter to smooth the fluctuations. **Figure 4c** demonstrates the moving average of the EEG power from **Figure 4b**. The features of rising and falling in the moving average power associated with eye close and open, respectively, can be detected by comparing the moving average power with a preset threshold. A threshold of 80 $(\mu V)^2$ was selected for edge detection of eyes open or close. This threshold can be chosen individually during user training.

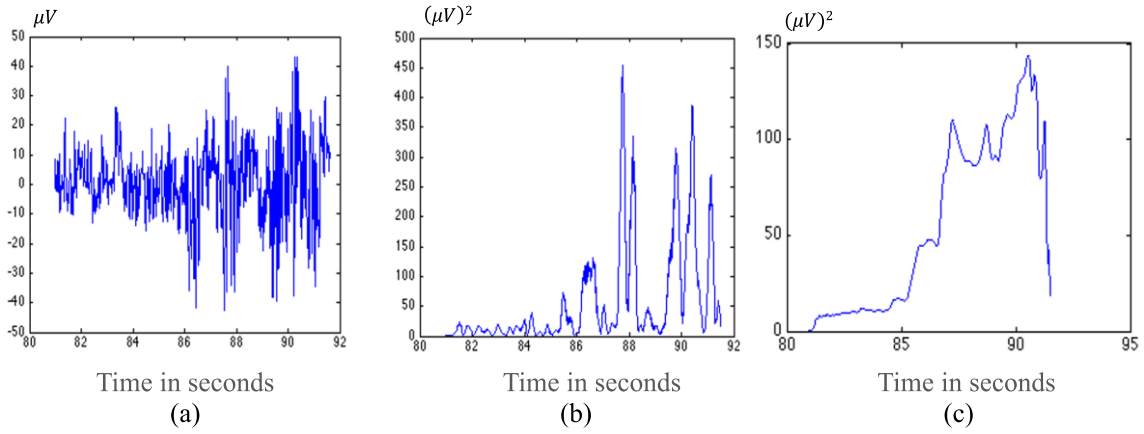

Figure 4. EEG alpha wave processed by the algorithm in **Figure 3**: **(a)** EEG signal, in μV, after bandpass filtering; **(b)** averaged EEG power, in $(\mu V)^2$, in a window size of $\frac{1}{10.5}$ s; **(c)** moving average of the EEG power in a 1.5-second window size.

2.2.2. Detection of fast eye blinking

Eye blinking produces a muscle artifact that can be detected by the electrodes located at AF3 and AF4 at the frontal lobe. Experimental data from the average of signals from AF3 and AF4 of a participant are illustrated in **Figure 5**. During the experiment, the participant blinked normally for the first 5 s, and then blinked fast for the next 5 s. It can be observed in **Figure 5** that the dominant frequency of the waveform is

associated with eye-blinking frequency. Each eye blink results in a significant pulse in both slow and rapid blinking. Counting the number of pulses in a pre-determined time window can be used to classify if a user is blinking abnormally fast, an indication of an intent.

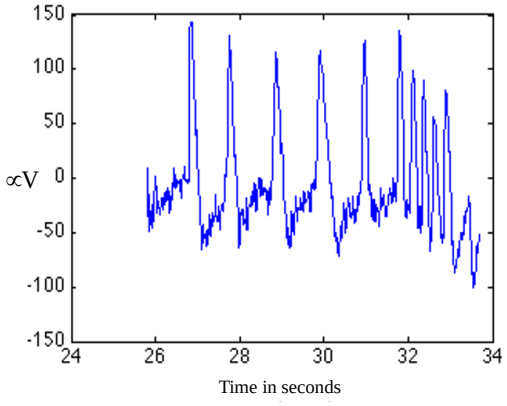

Figure 5. Data obtained from the frontal lobe during eye blinking experiment, normal blinking during the first 5 s and fast blinking for the next 5 s.

The eye-blinking detection algorithm is illustrated in the block diagram in **Figure 6**[17]. The EPOC EEG headset was used to obtain signals from the electrodes at AF3 and AF4, which were then high-pass filtered to remove the DC component. These filtered signals were averaged, as shown in **Figure 5**, to enhance signal quality. A rising-edge detector, with a threshold of 65 μV, was implemented on the host PC to count pulses from each eye blink. Fast eye blinking, defined as exceeding 5 blinks in 2 s, was considered a specific intent from the user.

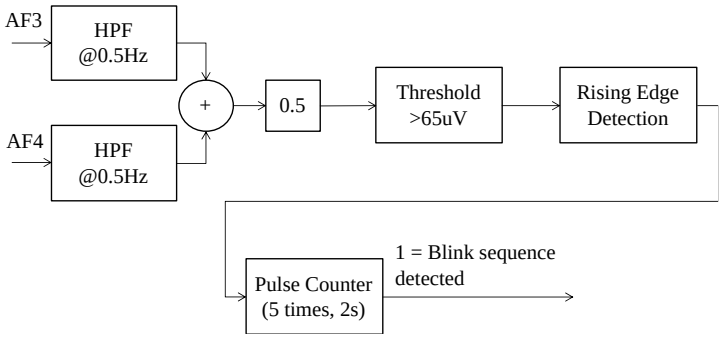

Figure 6. Block diagram of the eye blinking detection algorithm[17].

2.2.3. Detection of head rotation

The Emotiv EPOC headset includes two gyroscopes, providing angular velocity measurements in the azimuth and meridian axes. The gyroscope measurement obtained from the azimuth axis is used to determine the head rotation of the user. The angular position of the user's head relative to the calibrated center head position can be determined by the time integral of the gyroscope measurement obtained from the azimuth axis. Calibration for the initial position of the user's head is performed when the program first begins, and recalibration can be done at any time while the program is running. To reduce drift due to the sensor and numerical integration, clipping is applied by forcing the signal to zero when the user's head is close to the initial position[10]. The block diagram of the algorithm to determine the angular position of the user's head rotation is depicted in **Figure 7**[17].

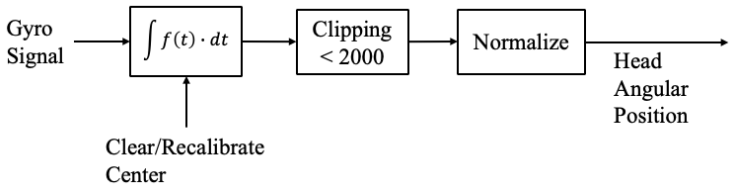

Figure 7. Block diagram of the algorithm to determine the angular position of the user's head[17].

2.3. Control schemes

Five features can be classified by using the signals acquired from the user through the Emotiv EPOC EEG headset: eye open and closure from the occipital alpha wave, head rotation left and right from the gyroscope in the azimuth axis, and fast eye blinking from muscle movement. These features are mapped to five different commands through a control scheme to navigate a robotic device. Another robotic device can be used with the same BCI system by switching to another control scheme dedicated to the device.

The commands employed in the control scheme for quadcopter navigation are described in the following[10]:

- Toggling the quadcopter to take off or land on the ground: a series of fast eye blinks (at least 5 blinks in 2 s).
- Moving forward: The user can control the quadcopter to move forward at a pre-set speed and altitude by closing and then re-opening their eyes. These sequential actions result in the rise (due to eye closure) and fall (due to eye opening) of the EEG alpha wave. The feature classifier in the BCI system detects these changes and triggers rising and falling edges in the control logic. The control scheme receives this logic to produce the control command for the quadcopter.
- Hovering: While the quadcopter is moving forward, the user can stop its motion by closing their eyes (rising edge). The final falling edge in this sequence is ignored to allow the user to reopen their eyes once the quadcopter has hovered, enabling them to keep their eyes open when the quadcopter is operating in the air.
- Turning left/right: Controlling the quadcopter to turn left or right was carried out using the angular position of the user's head by integrating the angular velocity measurement from the gyroscope in the azimuth axis with a calibration to centralize the user's head position. This angular position signal was then clipped, normalized, and mapped to the rotational speed of the quadcopter, allowing the user to turn the quadcopter in a small angle of rotation while maintaining the stability of the quadcopter.

A graphical user interface, as shown in **Figure 8a**, was displayed on the host PC to communicate the operational state of the quadcopter with the user.

The wheeled robot and the wheelchair in this study share the same control scheme, as both devices utilize identical control commands for operation. In this control scheme, the increased alpha wave activity detected over the occipital lobe (O1 and O2) during eye closure is used to initiate and cease movement of the robot or wheelchair. The commands used to move the quadcopter forward and maintain it hovering in the air are employed here to start and stop the wheeled robot or wheelchair, respectively. Rapid eye blinking, operationally defined as five blinks within two seconds detected over the frontal lobe (AF3 and AF4), is utilized to reverse the direction of the robot, allowing users to toggle between forward and backward movement. Head rotation, detected by the azimuth axis gyroscope using the same algorithm employed to navigate the quadcopter when turning left or right, is used to control the navigation of turns for the robot. The graphical user interface, depicted in **Figure 8b**, was developed to provide simple instructions to the user and offer visual feedback on the operational states of the robot[14].

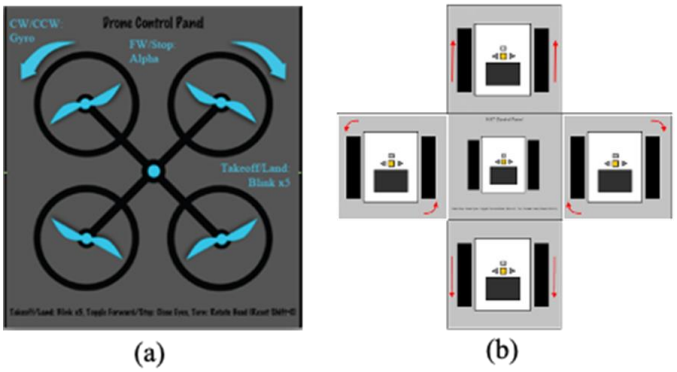

Figure 8. Graphical user interface for robotic device navigation, **(a)** for quadcopter navigation[17]; and **(b)** for wheeled robot and wheelchair navigation[18].

Two safety features have been implemented to manage events such as wireless signal loss and emergency landing or stopping[17,18]. The wireless connection between the Emotiv headset and the host PC may drop while the robot is in operation, prompting the implementation of a watchdog timer to monitor the connection. In the event of a connection timeout, the quadcopter will hover in place until the connection is re-established. Similarly, when operating the wheeled robot or wheelchair, the robot or wheelchair will come to a stop until the connection is re-established.

The landing process for the quadcopter is typically controlled by fast eye blinking. However, in case of an emergency, an emergency stop can be initiated by pressing any key on the keyboard. This action forces the quadcopter to land and remain grounded until another key is pressed. The emergency stop feature has also been implemented to halt the wheeled robot and wheelchair.

2.4. Robotic devices

Three robotic devices were used in this development: a quadcopter (Parrot AR.Drone, Parrot SA, France), a wheeled robot (LEGO Mindstorms NXT, The Lego Group, Denmark), and a wheelchair. The quadcopter communicates with the host PC via WiFi by establishing its access point and accepting control commands sent to one of the User Datagram Protocol (UDP) servers running on the device. The Nodecopter library, installed on the host PC, was used to send high-level commands (takeoff, land, forward) in Node.js. The Node.js script, a software package on the host PC, receives high-level commands (takeoff, land, forward, etc.) and passes them to the quadcopter over its WiFi network. The AR.Drone also features on-board stability control and an altitude mode for hovering in place. These features are crucial for the BCI user to maintain the quadcopter in the air without continuously managing their mental state. Visual feedback for remote operation is available via two cameras (front and down-facing) on the AR.Drone[17].

The LEGO Mindstorms NXT robot serves as a model of the wheelchair for user training. The device's original firmware was replaced with open-source firmware, simplifying the integration of signal processing with the robot's movements, as described by Smith[18]. Both the Emotiv EPOC headset and the NXT robot were wirelessly connected via Bluetooth to an Alienware laptop, which contained signal processing algorithms and facilitated the integration of neural signals into robotic actions[14].

The electric wheelchair was specifically designed for this application, employing a pair of DC motors controlled through Victor 884 motor controllers by an Arduino Uno microcontroller. The microcontroller receives commands such as forward, backward, turning left/right, and stop from the BCI control scheme on the host laptop PC through a USB cable. It then sends pulse-width modulation signals to the motor controllers to execute the desired tasks. **Figure 9**[18] illustrates the block diagram representing the connections of the wheelchair's components.

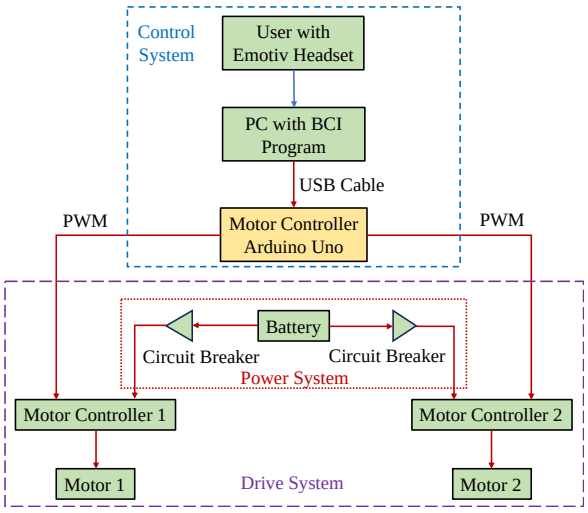

Figure 9. The block diagram illustrates the interconnection for the design of the wheelchair[18].

3. Experiments

The design of the BCI system incorporates signal processing for feature extraction and classification with control schemes, which is intended for navigating robotic devices. This system was implemented in Java and evaluated in two steps. The first set of experiments aimed to test the overall performance of the system, while the second set aimed to establish a calibration procedure and evaluate the accuracy and reliability of the design across multiple users. All experiments were approved by the Lafayette College Institutional Review Board.

3.1. Overall performance test

Overall system performance was assessed by instructing users to control the quadcopter, the LEGO robot, and the wheelchair through commands conveyed by eye open/closure, eye blinking, and head rotations while the responses were recorded by the robots. The recorded responses from the robots were compared with users' intents and classified into one of the four categories using the confusion matrix approach[10,14].

- True Positive (TP): the device responds correctly to the intended command.
- False Positive (FP): the device performs an action when the user is not intending to issue a command
- False Negative (FN): the device does not respond correctly to the intended command.
- True negative (TN): the device does not respond when there is no command.

The accuracy of the performance was quantified by

$$\mathrm{ACC} = \frac{\mathrm{TP}}{\mathrm{TP} + \mathrm{FP} + \mathrm{FN}} 100\% \tag{2}$$

where ACC represents the percentage accuracy. True negatives were not measured, as there is no specific event that can be counted as a true negative. During this test, the thresholds applied to classify users' intents were adjusted to determine the sensitivity of the system's performance to these thresholds.

3.2. Evaluation of the system performance across multiple users

In the second set of experiments, a test procedure involving training and testing was conducted with each individual participant over the two time points, with the second time point occurring within 48 h[19]. The results of the second-time test provide information about the participants' ability to retain the skills they learned from the first-time test. During the preparation for the experiment, measurements of the participant's head circumference and distance from nasion-inion were taken. Three dots were placed on the back of the participant's head using a washable marker: one at ten percent of the nasion-inion distance above the inion (position Oz), and the other two at five percent of the circumference on the left and right of Oz (positions O1

and O2 in **Figure 2**). After soaking all felt pads with a saline solution and placing them into electrode sensors on the headset, the headset was positioned so that the reference sensors made good contact with the scalp, and the O1 and O2 electrodes aligned with the dots drawn in the respective locations. Once the two references were established, impedance values were checked for the remainder of the electrodes.

The entire test consisted of three sequential steps: calibration, training, and navigation, as described below. Calibration involved determining the threshold values of each asynchronous signal within ten-second intervals for each participant. To analyze alpha activity, participants kept their eyes open for five seconds, closed their eyes, and relaxed for an additional five seconds. Facial muscle signals produced by rapid blinking were examined: participants relaxed for four seconds, then blinked five times within two seconds, followed by another four seconds of relaxation. Both processes were repeated three times to ensure signal consistency. The raw signals underwent post-processing in MATLAB and were analyzed to determine a threshold value. This threshold was defined based on a consistent value attained during the desired action or mental state only. For the alpha wave, raw signals were averaged, bandpass filtered between 8 to 13 Hz, and plotted along a smooth power curve, using the processing method described in the research of Garrison[17]. Based on the smooth power curve, the maximum rising derivative over a 2-second window (usually between 4.5 to 6.5 s) was calculated for each trial, and the average of these three values was used as the threshold. For all participants, the gyroscope threshold was set to 20% of the total possible turning radius detected by the gyroscope.

Following calibration, the accuracy of each of the three signals was tested to ensure that the signals were usable for the control of the LEGO NXT robot. Using the thresholds established during the initial calibration, a confusion matrix approach was employed to determine signal accuracy. For rapid blinking and alpha wave modulation, participants were instructed to "blink" or "close" their eyes 20 times, approximately every ten seconds, and the number of true positives (TPs), false positives (FPs), and false negatives (FNs) during this time were recorded. For head rotation, participants were instructed to turn left or right ten times in each direction, in a randomized order. Once again, the number of TPs, FPs, and FNs during this time were recorded. Percent accuracy, as calculated in Equation (2), was applied to determine the performance. If the accuracy of each signal was over 80%, participants moved on to the training portion, where they received visual feedback (robot actions) based on their commands. If the accuracy was less than 80%, then the threshold for that particular signal was re-calibrated, and the signal accuracy was re-determined. This re-calibration process could occur up to three times for each signal; however, if the accuracy failed to exceed 80% after three attempts, the threshold associated with the highest percent accuracy reached was used for the training and testing portions.

The training session involved a series of increasingly difficult tasks designed to teach users the basic controls of the BCI device. Each task was timed, and users were instructed to try to complete each task within 3 min. The time limits were calculated by taking into consideration the length of the task and the speed of the robot; the time limit was set to double the minimum time in which such a task could be accomplished. Errors, operationally defined as two or more wheels crossing the designated boundaries of the course, were recorded. Participants attempted each task eight times or until they completed it successfully three consecutive times, whichever came first. The three training tasks were as follows.

- Initiate movement of the robot in 10 s, or less.
- Navigate the robot forward 90 cm, reverse directions within the designated area, and travel backward the same distance until the robot crossed the starting line with all four wheels (38 s max completion time).
- Navigate the robot forward 90 cm, perform a 90° turn, travel forward 60 cm, and stop the robot within a 30 cm by 30 cm square area (55 s max completion time). The percentage of successful attempts out of the total number of attempts was determined for each task.

Following the training session, participants navigated an obstacle course, as shown in **Figure 10**, designed to simulate a realistic wheelchair environment. The course consisted of scaled-down tasks representing challenges encountered by wheelchair users in their daily lives. Obstacles included a ramp, stall, various right- and left-hand turns, and an emergency stopping point, all designed in accordance with the guidelines specified by the Americans with Disabilities Act[20]. Participants were instructed to start the robot, guide it down a ramp, make a scheduled stop within a designated area, continue navigating through the 'hallway,' enter a designated area (simulated bathroom stall), execute a full turn, and then exit the stall to complete the obstacle course. They were instructed to complete the course as quickly as possible with as few errors as possible. An 'error' was defined as two or more wheels crossing over a marked border, indicating that more than half of the robot was out of bounds. In such cases, the experimenter repositioned the robot to its previous location on the course, and the participant resumed completion of the obstacle course. The time to completion (excluding the time taken for repositioning or resetting the robot) and the number of errors committed throughout the course were determined through offline analysis of video recordings of participant performance.

After the completion of the task, participants were asked to return to the lab within 24–48 h for an additional training/testing session to examine their ability to control the device over time. The procedure for day two was the same as for day one, including calibration, accuracy calculation, training, and testing.

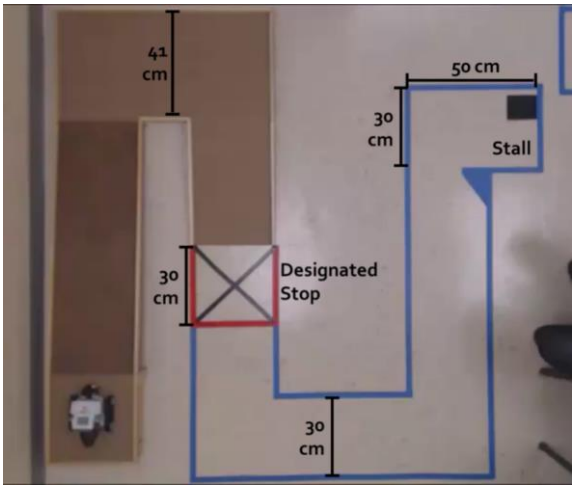

Figure 10. The obstacle course was constructed as a model of various features that wheelchair users may encounter on a daily basis, including a ramp (far left, robot is located at the top of the ramp), designated stop (red box at end of ramp), hallways including two left turns (blue), ending with an entrance into a bathroom stall. The course was designed to meet ADA regulations using the robot as a scaled-down model of a wheelchair[19].

4. Result and discussion

4.1. Results from the overall performance test

For the quadcopter test, a female college student followed the instructions (eye open/close and blinking) provided by the data collection personnel to navigate the quadcopter. As indicated in **Table 1**, the occipital alpha wave demonstrated high reliability at a threshold of 70 $(\mu V)^2$. Two threshold settings were employed for the blinking test. The results in **Table 1** suggest that a higher threshold improves true positives and reduces false positives. Consequently, the percentage of accuracy was higher when using a higher threshold setting.

The same test was conducted by a male student operating the LEGO NXT robot, and the results are presented in **Table 1**. The occipital alpha wave achieved an accuracy rate of 87.5% at a threshold of 30 $(\mu V)^2$, while blinking yielded an accuracy rate of 90.5% at a threshold of 130 µV. Similar to the results from the quadcopter test, higher thresholds are less likely to produce false positive and false negative responses

than lower thresholds. Additionally, the threshold settings required to achieve good accuracy in testing both devices were different. These differences may be attributed to variations in impedance between the scalp and the EEG headset. As a result, calibration is necessary for each individual user prior to using the BCI system.

Throughout the entire test, the threshold for gyroscope sensitivity remained consistent for all participants at 20% of the maximum rotation possible in each direction.

After the completion of the task, participants were asked to return to the lab within 24–48 h for an additional training/testing session to examine their ability to control the device over time. The procedure for day two was the same as for day one, including calibration, accuracy calculation, training, and testing.

Table 1. Accuracy of alpha wave and blink test with different threshold settings.

Threshold/signal	TP	FP	FN	Accuracy (%)
Quadcopter test				
70 $(\mu V)^2$/alpha	41	0	0	100
65 µV/blink	9	5	2	56.3
70 µV/blink	11	4	2	64.7
LEGO NXT robot test				
25 $(\mu V)^2$/alpha	27	12	5	61.4
30 $(\mu V)^2$/alpha	21	1	2	87.5
120 µV/blink	19	0	4	82.6
130 µV/blink	19	0	2	90.5

4.2. Results from the evaluation of system performance across multiple users

Twenty healthy adults (8 males and 12 females), between 18 and 29 years of age (Mean ± SD: 21.0 ± 2.2 years), participated in the study to examine the effectiveness of navigating a Lego NXT robot with a wireless, hybrid BCI device. Individuals with head or neck injuries or diagnosed neurological conditions were excluded from this study. Following the completion of the study with the Lego robot, a single participant attempted to operate an electric wheelchair designed in the laboratory specifically for use with this hybrid BCI device.

4.2.1. Alpha wave calibration

The alpha wave was calibrated across three trials, with up to three calibrations performed in a single trial. The trial was considered complete once an accuracy rate of 80% or above was recorded, or a maximum of three calibration attempts were completed. The mean alpha wave amplitude was determined under two conditions: eyes open (EO) and eyes closed (EC), for each participant. The percent increase in amplitude during the eyes closed condition compared to the eyes open condition was calculated for each participant as

$$\text{Increase} = \frac{\text{EC} - \text{EO}}{\text{EO}} 100\% \quad (3)$$

Dependent *t*-tests for each participant were performed to examine the change in alpha amplitude across the two days of testing. There were statistically significant differences in amplitude between EO (day 1, M = 4.27, SD = 1.26; day 2, M = 3.86, SD = 0.94) and EC (day 1, M = 10.24, SD = 4.73; day 2, M = 11.21, SD = 5.19) on both day 1, $t(18) = -5.41$, $p < 0.001$, and day 2, $t(16) = -6.24$, $p < 0.001$. However, there was no statistical difference in the percent increase of the alpha wave across days (M_{Day1} = 166.53%, SD_{Day1} = 131.02; M_{Day2} = 192.53%, SD_{Day2} = 127.36), $t(16) = -1.19$, $p = 0.25$.

4.2.2. Threshold accuracy

The accuracy for each threshold ultimately used in the training and testing of the three parameters (alpha, blinking, and gyroscope) was calculated and compared between days one and two. The mean

threshold accuracies for each parameter on both days are reported in **Table 2**. There were no significant differences between the two days for alpha wave threshold accuracy, $t(16) = -0.84$, $p = 0.42$; blinking threshold accuracy, $t(16) = 1.29$, $p = 0.21$; or gyroscope accuracy, $t(16) = 0.60$, $p = 0.56$.

Table 2. Threshold accuracies for BCI robot controls.

	Day 1		**Day 2**	
Parameter	***M***	***SD***	***M***	***SD***
Alpha wave	76.27%	10.20	78.85%	11.02
Blinking	87.13%	11.24	82.68% 94.57%	13.70
Gyroscope	13.70%	5.04		3.95

4.2.3. Training

Three different training tasks were utilized: initiating movement (task 1), forward/backward movement (task 2), and completing a 90° turn (task 3). Training was considered complete when the participant successfully completed three consecutive trials, or a maximum of eight trials were performed. Once the maximum number of trials was attempted, the participant moved on to the next training task until all tasks were completed. Training performance was measured as the percentage of successful attempts out of the total attempts made across the two days of training.

There were no significant differences between the two days for task 1 (day 1, $M = 87.98\%$, $SD = 14.46$; day 2, $M = 95.20\%$, $SD = 11.48$), $t(16) = -1.45$, $p = 0.08$; task 2 (day 1, $M = 60.97\%$, $SD = 21.71$; day 2, $M = 73.06\%$, $SD = 26.77$), $t(16) = -1.57$, $p = 0.07$; or task 3 (day 1, $M = 57.01\%$, $SD = 21.71$; day 2, $M = 63.24\%$, $SD = 28.60$), $t(16) = -0.56$, $p = 0.29$.

4.2.4. Obstacle course testing

A dependent *t*-test was performed to examine the time taken to complete the course and the number of errors committed during completion. No statistically significant differences were found for time (day 1, $M = 137.60$ s, $SD = 37.00$; day 2, $M = 155.85$ s, $SD = 72.57$; $t(12) = -1.01$, $p = 0.33$) or errors (day 1, $M = 1.46$, $SD = 1.85$; day 2, $M = 2.69$, $SD = 3.40$; $t(12) = -1.23$, $p = 0.24$). Overall, 53.85% of participants on day 1 and 64.71% on day 2 were able to successfully complete the obstacle course's emergency stop component (i.e., stopping the robot within the 30 cm by 30 cm square on their first attempt). A Fisher's Exact test demonstrated that successful completion of the designated stop was not dependent on the day of testing; individuals performed equally well on day 2 as they did on day 1 of testing.

A multiple linear regression analysis was performed to understand how much variance in obstacle course performance (i.e., time) could be explained by measures of alpha wave increase, threshold accuracy for all three parameters, and responses to survey questions. A separate multiple regression was performed for each day of testing. Results from these analyses can be found in **Table 3**. Overall, it was found that 31.3% of the variance in course time on day 1 could be explained by the variance in accuracy of the alpha threshold, and an additional 24.7% of variance could be explained by levels of excitement before beginning the experiment. On day 2, 59.4% of the variance in course time could be explained by levels of frustration.

Table 3. Multiple regression analysis of variables affecting the obstacle course performance.

	Time to complete maze		
	Day 1		
	R^2	ΔR^2	***F* ratio**
Model 1			
Alpha Threshold Accuracy	0.313	-	5.015*
Model 2			
Alpha Threshold Accuracy Excitement	0.560	0.247	6.353**
	Day 2		
	R^2	ΔR^2	***F* ratio**
Model 1			
Frustration	0.594	-	19.053***

* $p < 0.05$, ** $p < 0.02$, *** $p < 0.001$.

4.2.5. Wheelchair testing

One female college student, after two days of individual training, participated in the preliminary test for the wheelchair. Since the wheelchair uses the same control scheme as the LEGO NXT robot, the same threshold settings for the participant in the LEGO NXT robot test were adopted for the wheelchair test. In this test, the participant followed instructions to start and stop the wheelchair, make left and right turns, and reverse direction. Each operation was repeated 20 times. The responses from the wheelchair were recorded and compared with the user's intents, classified into one of the four categories using the confusion matrix approach – the same approach described in the systems integration test. The test results are summarized in **Table 4**. High accuracy rates in all operation tests suggested that the systematic training with the LEGO NXT robot provided a valuable path for users to operate the BCI-controlled wheelchair effectively.

Table 4. Preliminary test results with the wheelchair.

Control command	**TP**	**FP**	**FN**	**Accuracy (%)**
Start/stop	20	0	0	100
Right turn	20	0	0	100
Left turn	17	0	3	85
Reverse direction	18	1	1	90

5. Conclusion

This paper presents the design of an asynchronous BCI system capable of controlling three different robotic devices by selecting dedicated control schemes for each device without requiring major design changes in the BCI system or additional training for users. An inexpensive EEG headset (EPOC, EMOTIV System, San Francisco, CA) was used for signal acquisition in this BCI system, enhancing affordability for a broader user base. The EEG headset captures the EEG alpha wave (associated with eye open/close), artifacts from muscle movement (caused by eye blinking), as well as gyroscope signals related to slow head rotation and transmits these signals wirelessly to the host PC. In the host PC, these signals are processed to identify users' intentions for robot operation. Given that eye open/close, eye blinking, and head rotations are natural human motions, users can easily learn to operate this BCI system effectively without the need for time-consuming intensive training.

A quadcopter (Parrot AR.Drone, Parrot SA, France) and a wheeled robot (LEGO Mindstorms NXT, The Lego Group, Denmark) were used to test the integration of the BCI system. The results suggested that

the accuracy of the BCI can be adjusted by calibrating the thresholds for feature classification. Higher thresholds would result in higher percentage accuracies. In addition, individual calibration is essential to achieve overall good accuracy.

A series of experiments was conducted with 20 participants to investigate how BCI performance is impacted by training and time. The threshold settings in the BCI system were determined for each individual participant during calibration. After calibration, a series of tasks was provided to train the participants in operating the robot effectively. Once the training was completed, 17 out of the 20 participants were able to navigate the LEGO robot through an obstacle course, which consisted of scaled-down tasks mimicking daily challenges encountered by wheelchair users, with a small number of errors. A two-day repeated test in this study demonstrated that participants performed equally well on the first and second days of testing, with the second day occurring at least 24 h later.

A preliminary test of the wheelchair was conducted with one participant after receiving full training using the LEGO NXT robot. The results from this test supported the effectiveness of the training, enabling the user to operate the BCI system with high accuracy. Further study, involving more participants for testing, is needed to evaluate the overall performance of the BCI system with the wheelchair.

In conclusion, the BCI system and the systematic training procedure presented in this paper contribute valuable insights toward our long-term goal of developing a user-friendly and low-cost BCI system capable of controlling various robotic devices based on users' choices and needs. The success of this development has the potential to enhance user autonomy, ultimately leading to an improved overall quality of life.

Author contributions

Conceptualization, YCY and LG; methodology, HG, YCY, LG and BS, software, HG and BS; validation, HG, AB, AG and BS; formal analysis, AG, HG and BS; investigation, HG, AG, BS and AB; writing—original draft preparation, YCY; writing—review and editing, YCY and LG; project administration, YCY and LG; funding acquisition, YCY and LG. All authors have read and agreed to the published version of the manuscript.

Funding

This work was supported in part by the Lafayette College faculty development grant and the National Science Foundation under Grant ECCS-1126707.

Conflict of interest

The authors declare no conflict of interest.

References

1. McFarland DJ, Wolpaw JR. Brain-computer interfaces for communication and control. Communications of the ACM. 2011; 54(5): 60-66. doi: 10.1145/1941487.1941506
2. Shih JJ, Krusienski DJ, Wolpaw JR. Brain-Computer Interfaces in Medicine. Mayo Clinic Proceedings. 2012; 87(3): 268-279. doi: 10.1016/j.mayocp.2011.12.008
3. Hehenberger L, Kobler RJ, Lopes-Dias C, et al. Long-Term Mutual Training for the CYBATHLON BCI Race with a Tetraplegic Pilot: A Case Study on Inter-Session Transfer and Intra-Session Adaptation. Frontiers in Human Neuroscience. 2021; 15. doi: 10.3389/fnhum.2021.635777
4. Xu B, Li W, Liu D, et al. Continuous Hybrid BCI Control for Robotic Arm Using Noninvasive Electroencephalogram, Computer Vision, and Eye Tracking. Mathematics. 2022; 10(4): 618. doi: 10.3390/math10040618
5. Bai X, Li M, Qi S, et al. A hybrid P300-SSVEP brain-computer interface speller with a frequency enhanced row and column paradigm. Frontiers in Neuroscience. 2023; 17. doi: 10.3389/fnins.2023.1133933
6. Robinson N, Mane R, Chouhan T, et al. Emerging trends in BCI-robotics for motor control and rehabilitation. Current Opinion in Biomedical Engineering. 2021; 20: 100354. doi: 10.1016/j.cobme.2021.100354

7. Li Z, Li B, Luo W, et al. Design and Implementation of P300 Brain-Controlled Wheelchair with a Developed Wireless DA Converter. International Journal of Computers & Technology. 2023; 23: 93-104. doi: 10.24297/ijct.v23i.9485
8. Sellers EW, Vaughan TM, Wolpaw JR. A brain-computer interface for long-term independent home use. Amyotrophic Lateral Sclerosis. 2010; 11(5): 449-455. doi: 10.3109/17482961003777470
9. Ai J, Meng J, Mai X, et al. BCI Control of a Robotic Arm Based on SSVEP With Moving Stimuli for Reach and Grasp Tasks. IEEE Journal of Biomedical and Health Informatics. 2023; 27(8): 3818-3829. doi: 10.1109/jbhi.2023.3277612
10. Yu YC, Garrison H, Battison A, et al. Control of a Quadcopter with Hybrid Brain-Computer Interface. 2019 IEEE International Conference on Systems, Man and Cybernetics (SMC). Published online October 2019. doi: 10.1109/smc.2019.8914579
11. Chen W, Chen SK, Liu YH, et al. An Electric Wheelchair Manipulating System Using SSVEP-Based BCI System. Biosensors. 2022; 12(10): 772. doi: 10.3390/bios12100772
12. Yu Y, Liu Y, Jiang J, et al. An Asynchronous Control Paradigm Based on Sequential Motor Imagery and Its Application in Wheelchair Navigation. IEEE Transactions on Neural Systems and Rehabilitation Engineering. 2018; 26(12): 2367-2375. doi: 10.1109/tnsre.2018.2881215
13. Aljalal M, Djemal R, Ibrahim S. Robot Navigation Using a Brain Computer Interface Based on Motor Imagery. Journal of Medical and Biological Engineering. 2018; 39(4): 508-522. doi: 10.1007/s40846-018-0431-9
14. Yu YC, Smith B, Goreshnik A, et al. Design of an Affordable Brain-Computer Interface for Robot Navigation. 2019 14th IEEE Conference on Industrial Electronics and Applications (ICIEA). Published online June 2019. doi: 10.1109/iciea.2019.8833813
15. Corbit V, Gabel LA, Yu YC. Improving Mu Rhythm Brain-Computer Interface Performance by Providing Specific Instructions for Control. 2013 39th Annual Northeast Bioengineering Conference. Published online April 2013. doi: 10.1109/nebec.2013.166
16. Tran Y, Boord P, Middleton J, et al. Levels of brain wave activity (8–13 Hz) in persons with spinal cord injury. Spinal Cord. 2004; 42(2): 73-79. doi: 10.1038/sj.sc.3101543
17. Garrison H. Application of the Brain-Computer Interface to Robotics Control [Bachelor's thesis]. Lafayette College; 2015.
18. Smith B. Design of a Wheelchair for Use with a Brain-Computer Interface [Bachelor's thesis]. Lafayette College; 2017.
19. Goreshnik A. Accuracy and Reliability Study of Brain-Computer Interface Robot Navigation [Bachelor's thesis]. Lafayette College; 2017.
20. 2010 ADA Standards for Accessible Design. Available online: https://www.ada.gov/law-and-regs/design-standards/2010-stds/ (accessed on 15 October 2016).